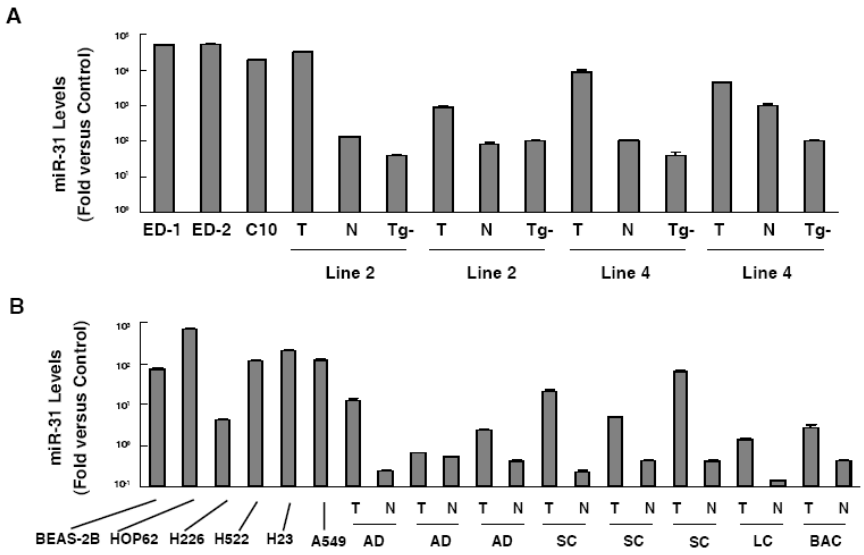

Supplemental Fig. 1. Validation of miR-31 expression by real-time RT-PCR assays performed on the indicated cell lines as well as on malignant and adjacent normal lung tissues from murine cyclin E transgenic lines and on paired normal-malignant human lung tissues. **A**) Independent real-time RT-PCR assays for miR-31 in murine ED-1, ED-2, C10 cells and murine cyclin E transgenic malignant versus normal lung tissues with symbols depicting T, malignant transgenic lung tumor; N, adjacent normal murine transgenic lung tissue; and Tg-, murine non-transgenic FVB normal lung tissue. Results represented the fold changes of miR-31 expression relative to sno-135 (control small RNA). **B**) Independent real-time RT-PCR assays for miR-31 were performed on RNA derived independently from BEAS-2B, HOP62, H226, H522, H23 and A549 cells as well as from paired human normal-malignant lung tissues, with symbols depicting T, malignant lung tumor; N, adjacent normal lung tissue; AD, adenocarcinoma; LC, large cell carcinoma; BAC, bronchioalveolar carcinoma; and SC, squamous cell carcinoma. Results represented the fold of miR-31 relative to RNU6B (control small RNA). Standard deviation bars are displayed.

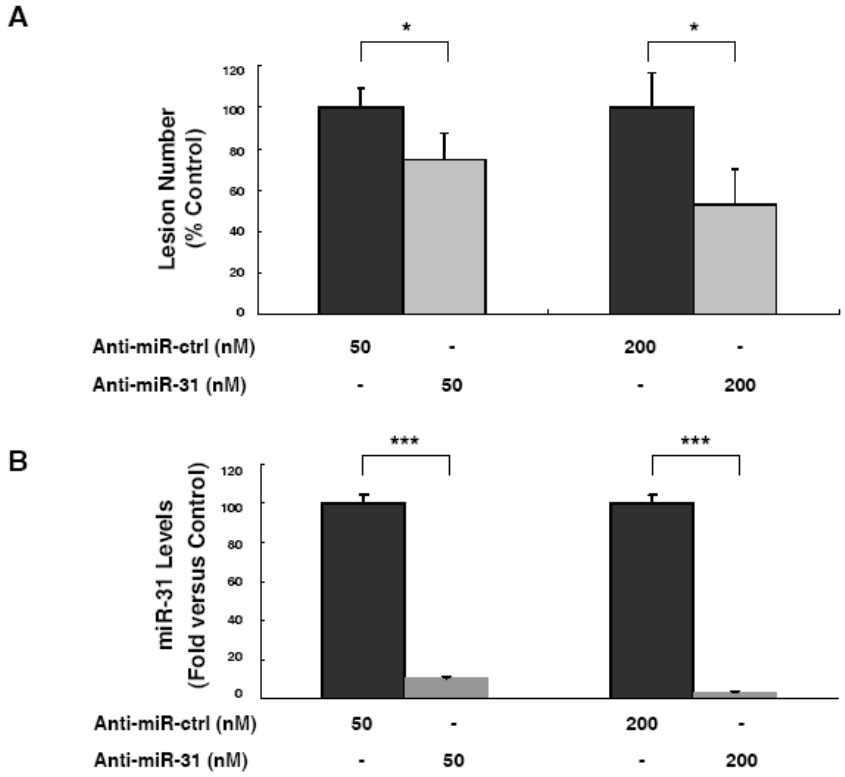

Supplemental Fig. 2. The dose-dependent knock-down of miR-31 leads to repression of *in vivo* lung tumorigenicity in the indicated transfected ED-1 cells following FVB mouse tail-vein injections. The bars in panel A represent the percentage of lung lesions relative to mice injected with anti-miR-ctrl (control) transfected cells, as described in the Methods and Materials. Panel B displays the miR-31 expression levels for transfectants. The symbols displayed are: *, $P < 0.05$ and ***, $P < 0.0001$. Standard error bars are displayed in panel **A** and standard deviation bars are displayed in panel **B**. The t-tests presented are one tail (panel **A**) and two tail (panel **B**), respectively.

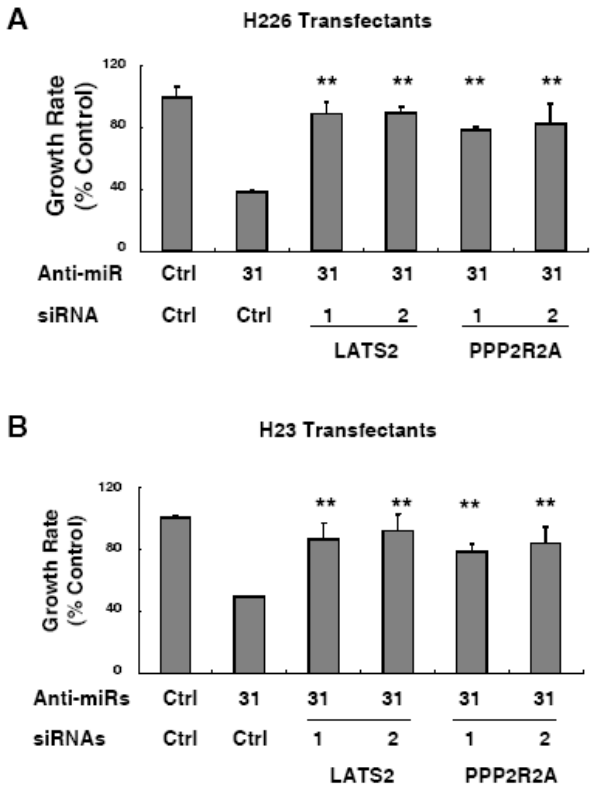

Supplemental Fig. 3. The effect on proliferation and on LATS2 and PPP2R2A expression in human lung cancer cells following engineered repression of miR-31. The panels display **A**) H226 cells and **B**) H23 cells that exhibit growth suppression following anti-miR-31 transfection of these cells. This effect was antagonized by either LATS2 or PPP2R2A siRNA targeting transfections performed 48 hours after anti-miR-31 transfection. Two independent siRNAs were each used to target LATS2 or PPP2R2A. The symbols displayed are: ** and $P < 0.01$. Standard deviation bars are displayed

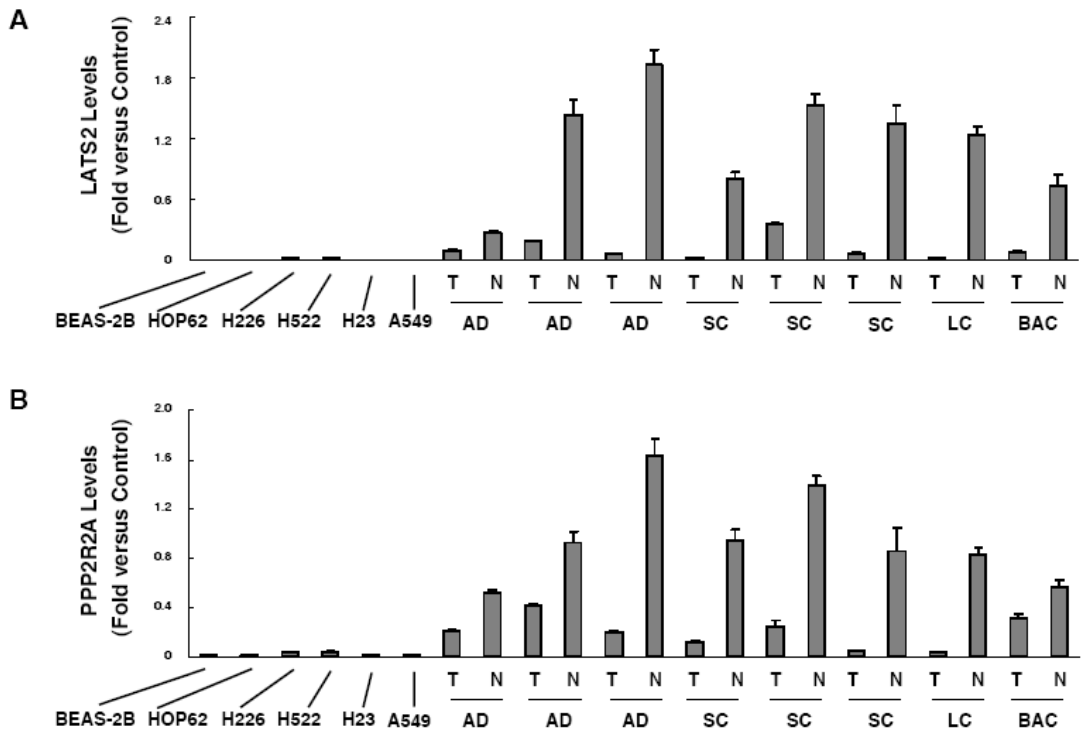

Supplemental Fig. 4. Validation of **A**) LATS2 and **B**) PPP2R2A expression by real-time RT-PCR assays performed on RNA derived independently from BEAS-2B, HOP62, H226, H522, H23 or A549 cells as well as from paired human normal-malignant lung tissues, with symbols depicting T, malignant lung tumor; N, adjacent normal lung; AD, adenocarcinoma; LC, large cell carcinoma; BAC, bronchioalveolar carcinoma; and SC, squamous cell carcinoma. Results represented the fold of LATS2 or PPP2R2A expression relative to GAPDH. Standard deviation bars are displayed.